ORNL/TM-2021/2269

Radiation Shielding Analysis of Niowave's Uranium Target Assembly 2 (UTA-2) Facility for Molybdenum-99 Production

Noel B. Nelson
Michael B. R. Smith
Zain Karriem
Jorge Navarro
Chad P. Denbrock
Robert N. Wahlen
Terry L. Grimm

July 2022

OAK RIDGE
National Laboratory

ORNL IS MANAGED BY UT-BATTELLE LLC FOR THE US DEPARTMENT OF ENERGY

DOCUMENT AVAILABILITY

Reports produced after January 1, 1996, are generally available free via US Department of Energy (DOE) SciTech Connect.

Website www.osti.gov

Reports produced before January 1, 1996, may be purchased by members of the public from the following source:

National Technical Information Service
5285 Port Royal Road
Springfield, VA 22161
Telephone 703-605-6000 (1-800-553-6847)
TDD 703-487-4639
Fax 703-605-6900
E-mail info@ntis.gov
Website http://classic.ntis.gov/

Reports are available to DOE employees, DOE contractors, Energy Technology Data Exchange representatives, and International Nuclear Information System representatives from the following source:

Office of Scientific and Technical Information
PO Box 62
Oak Ridge, TN 37831
Telephone 865-576-8401
Fax 865-576-5728
E-mail reports@osti.gov
Website https://www.osti.gov/

This report was prepared as an account of work sponsored by an agency of the United States Government. Neither the United States Government nor any agency thereof, nor any of their employees, makes any warranty, express or implied, or assumes any legal liability or responsibility for the accuracy, completeness, or usefulness of any information, apparatus, product, or process disclosed, or represents that its use would not infringe privately owned rights. Reference herein to any specific commercial product, process, or service by trade name, trademark, manufacturer, or otherwise, does not necessarily constitute or imply its endorsement, recommendation, or favoring by the United States Government or any agency thereof. The views and opinions of authors expressed herein do not necessarily state or reflect those of the United States Government or any agency thereof.

ORNL/TM-2021/2269

Nuclear Energy and Fuel Cycle Division

RADIATION SHIELDING ANALYSIS OF NIOWAVE'S URANIUM TARGET ASSEMBLY 2 (UTA-2) FACILITY FOR MOLYBDENUM-99 PRODUCTION

Noel B. Nelson
Michael B. R. Smith
Zain Karriem
Jorge Navarro
Chad P. Denbrock
Robert N. Wahlen
Terry L. Grimm

July 2022

Prepared by
OAK RIDGE NATIONAL LABORATORY
Oak Ridge, TN 37831-6283
managed by
UT-BATTELLE LLC
for the
US DEPARTMENT OF ENERGY
under contract DE-AC05-00OR22725

CONTENTS

EXECUTIVE SUMMARY 1
1. INTRODUCTION 1
2. BACKGROUND AND GOALS 2
3. MATERIALS AND METHODS 3
    3.1 MCNP MODEL 3
    3.2 MAVRIC LBE SOURCE 8
        3.2.1 Photons 8
        3.2.2 Neutrons 11
        3.2.3 MAVRIC Fission Source 15
4. RESULTS 19
    4.1 OCCUPATIONAL DOSE RATE RESULTS 21
    4.2 OBSERVATIONS AND RECOMMENDATIONS 23
5. CONCLUSION 24
6. REFERENCES 25
APPENDIX A. TABULATED DOSE RATES A-2

EXECUTIVE SUMMARY

Niowave is seeking to develop a commercial medical isotope production process using a low-enriched uranium accelerator-driven subcritical reactor (ADSR) system to produce molybdenum-99. As part of the US Department of Energy national laboratory support to develop low enriched uranium molybdenum-99 production technologies, Oak Ridge National Laboratory is providing research and development resources to assist Niowave in the design and licensing process of its technology. The goals of this work under the radiation shielding task are to assist Niowave in developing a methodology and framework for efficient radiation shielding simulations of their Uranium Target Assembly 2 facility and to provide preliminary radiation shielding calculations and design recommendations for the facility.

The SCALE/MAVRIC package was selected to perform radiation shielding calculations because it has an adjoint accelerated radiation transport framework ideal for deep penetration and complex radiation shielding problems. The package does not have an electron transport physics capability, however, so a photon-neutron source reduced order model (ROM) was developed to simplify the original electron-photon-neutron particle physics problem. In other words, this method decouples the electron-bremsstrahlung accelerator target physics from the (photon-neutron) subcritical reactor assembly physics and splits them into two separate calculations. Calculating the target source in this manner should yield further acceleration benefits by removing a third of the physics calculations; however, accurately reproducing those target physics is a complex problem.

A preliminary target ROM methodology was developed in this work for both a photon and neutron target source. When compared with results from the Monte Carlo N-Particle Transport triple-particle physics model, the neutron target source ROM dose profile still has several discrepancies that need further investigation. The photon target source ROM is highly applicable to dose profiles in the direction parallel to the electron beam, which dominate dose contributions to the facility. Photon losses in directions perpendicular to the electron beam might need to be better accounted for since they are amplified by photofission in the fuel.

Preliminary facility calculations suggest that operational areas on the ground floor near the ADSR should be controlled and that additional shielding at the hall entryways could also be warranted. The majority of the rest of the facility can be classified as an *uncontrolled area* (i.e., areas are <0.002 rem/hour). Several other more general recommendations were made based on personnel safety, access control, and other sources of radiation that should be investigated (e.g., accelerator beamline radiation and activation products).

1. INTRODUCTION

Ever since the design of the first civilian commercial nuclear power station in Shippingport, Pennsylvania, in 1957, the nuclear industry has sought more efficient, secure, economical, and safe reactor designs for both power and medical isotope production purposes. Recently, the majority of international focus has been on investing in advanced nuclear reactors (WNA September 2020) and small modular reactors (WNA September 2020) to assist in meeting greenhouse gas emission reduction goals and in arresting climate change. However, there has also been a strong interest by the US Department of Energy (DOE) National Nuclear Security Administration (NNSA) to support commercial production of the medical isotope Mo-99 without using highly enriched uranium (or uranium enriched to 20% U-235 or greater) (NNSA 2019) in an effort to maintain modern international safeguard limits (IAEA 2001).

One way to meet medical isotope production efforts is through an accelerator-driven subcritical reactor (ADSR) with a photoneutron conversion target source (Makarashvili, Chemerisov, and Micklich 2012).

Other applications for accelerator-driven photoneutron sources include radiotherapy (Tatari and Ranjbar 2014) and transmutation of long-lived nuclear waste actinides (He 2015). Niowave, inc, is designing an ADSR system for the mission of Mo-99 medical isotope production. As part of the NNSA laboratory support, Oak Ridge National Laboratory is assisting Niowave with the development, design, and efficient modeling methodologies for the radiation shielding and reactor systems. This report focuses on the results of the radiation shielding analysis.

2. BACKGROUND AND GOALS

The Uranium Target Assembly 2 (UTA-2) Airport Facility is the location of the second Niowave brick-and-mortar site, where isotope production and considerations for occupational and public safety are paramount in nuclear facility licensing under the US Nuclear Regulatory Commission (NRC). Given the radiological implications of various components of the facility (i.e., accelerator, reactor, lead bismuth eutectics [LBEs]), nuclear analysis is required to estimate safe operational conditions for onsite personnel. The goal of this report is to calculate and analyze the radiation dose fields cast by operational equipment in the UTA-2 facility and develop radiation shielding design recommendations.

The primary source of radiation at the UTA-2 facility will be the ADSR system. Niowave's ADSR system will operate using a 20 MeV, 7 kW linear accelerator (LINAC) electron beam system in combination with an LBE target and a combined natural uranium (NU) and low-enriched uranium (LEU) subcritical reactor (Figure 1).

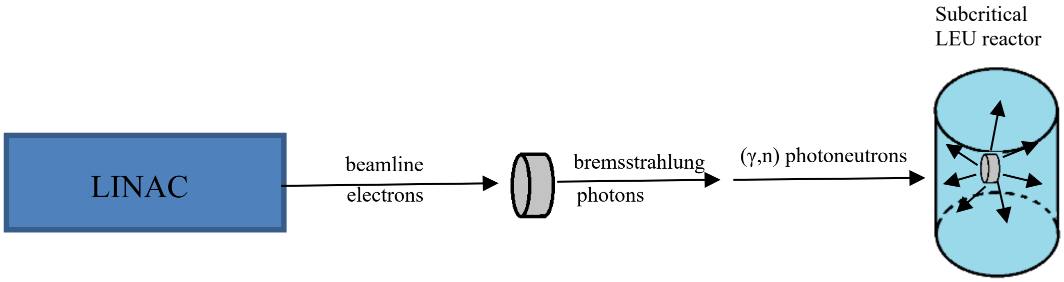

Figure 1: Schematic of the Niowave subcritical reactor system.

The Niowave ADSR works by creating bremsstrahlung photon radiation from relativistic electrons as they interact with the LBE target. The photons are then scattered and absorbed by the high-atomic-number (high-Z) materials within the LBE, which produce neutrons in photonuclear reactions for photon energies above the 6.5 MeV threshold energies according to historical data (IAEA 1974). Photoneutrons are then moderated by light water and multiplied within the NU/LEU fuel of the reactor. Unlike traditional research and power fission reactor systems, an ADSR is inherently safer than a critical nuclear reactor system because the neutron population will never reach either a critical or supercritical state ($k_{\text{eff}} \geq 1$). Yet it will still produce a reasonable concentration of fission products, which after some reprocessing, will yield Mo-99 (Bencomo 2016) and other commercially viable radioisotopes.

Although the criticality risks are much smaller, the radiation fields created during operation of the ADSR and during reprocessing the spent fuel will not be insignificant to the operators, and these fields must be safely controlled for operational safety and licensing purposes. Another goal of this work is to develop a reduced order model (ROM) and an efficient radiation shielding methodology for Niowave such that they can verify dose estimations of their facility using minimal computation resources. Such an ROM would accelerate facility dose calculations and quickly approximate the electron-to-photon-to-neutron conversion physics outlined in Figure 1.

3. MATERIALS AND METHODS

Early optimization work was performed using Monte Carlo N-Particle (MCNP) coupled electron-photon-neutron radiation transport simulations of the UTA-2 ADSR core. The core is a 13 × 13 cubic assembly of uranium oxide pins of two enrichments. The outer layer of pins is made of natural uranium, and the inner layer is 9.75% U-235. A schematic of the core is displayed in Figure 2.

Additionally, the pins are clad with aluminum, and the beamline and inner containment vessel are made of stainless steel. Specific dimensions and other details of the core are available on request from Niowave.

3.1 MCNP MODEL

The MCNP model of the UTA-2 ADSR core uses a multiphysics Monte Carlo radiation transport approach to calculate the effective dose from the leakage of photons and neutrons from the ADSR based on an initial incident flux of electrons from the LINAC. The full LINAC is not modeled, and the electron source is merely treated as a monodirectional pencil beam of 20 MeV electrons. This model requires significant computational resources to calculate and is best performed on a high-performance computing cluster.

To reduce computation times, it was decided that a ROM using only a photo-neutron LBE source should be developed using the SCALE package. MAVRIC (part of SCALE) provides an accelerated method for adjoint-driven Monte Carlo calculations which greatly accelerates deep penetration problems such as this. However, MAVRIC does not have an electron transport physics package, thus MCNP was required to develop the appropriate initial source term. In other words, the SCALE ROM is designed to take a coupled set of three steady-state, radiation transport equations (Equations [1–3]) solved by stochastic principles in MCNP and reduce it to two (Equations [2–3]) in SCALE.

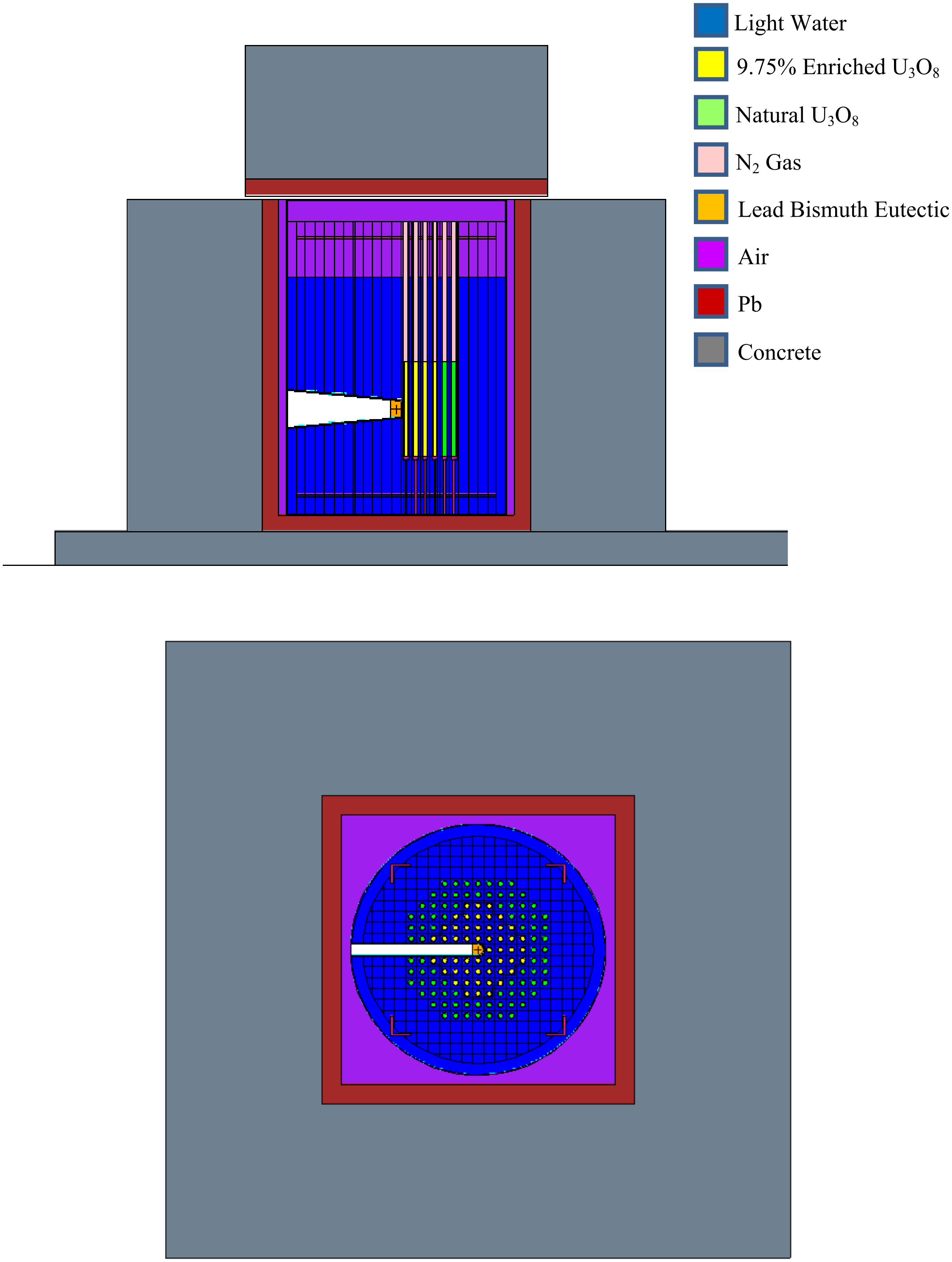

Figure 2: Vertical slice (top) and horizontal slice (bottom) of the UTA-2 ADSR core MCNP model. The dimensions of the UTA-2 assembly are available upon request from Niowave, Inc.

$$\begin{aligned}\hat{\Omega}\cdot\nabla\psi_{\mathrm{e}}(r,E,\hat{\Omega}) + \sigma_{\mathrm{t}}\psi_{\mathrm{e}}(r,E,\hat{\Omega}) &= \int_0^\infty\int_0^{2\pi}\int_{-1}^{1}\sigma_{\mathrm{s}}(E'\to E,\mu_0)\times \\ &\psi_{\mathrm{e}}(\mu',\varphi',E')d\mu'd\varphi'dE' + \frac{\alpha}{2}\left\{\frac{\partial}{\partial\mu}\left[(1-\mu^2)\frac{\partial\psi_{\mathrm{e}}(r,E,\hat{\Omega})}{\partial\mu}\right]+\frac{1}{1-\mu^2}\frac{\partial^2\psi_{\mathrm{e}}(r,E,\hat{\Omega})}{\partial\varphi^2}\right\} \\ &+\frac{\partial}{\partial E}\left[S\psi_{\mathrm{e}}(r,E,\hat{\Omega})\right] + Q_{\mathrm{e}}(r,E,\hat{\Omega})\end{aligned} \tag{1}$$

$$\begin{aligned}\hat{\Omega}\cdot\nabla\psi_{\mathrm{p}}(r,E,\hat{\Omega}) + \mu_{\mathrm{t}}(r,E)\psi_{\mathrm{p}}\left(r,E,\hat{\Omega}\right) &= \int_0^\infty\int_{4\pi}\mu_{\mathrm{s}}\left(E'\to E,\hat{\Omega}'\to\hat{\Omega}\right)\psi_{\mathrm{p}}\left(r,E',\hat{\Omega}'\right)d\hat{\Omega}'dE' + \\ &R_{\mathrm{pf}}\left(r,E,\hat{\Omega}\right) + Q_{\mathrm{p}}\left(r,E,\hat{\Omega}\right),\end{aligned} \tag{2}$$

$$\begin{aligned}\hat{\Omega}\cdot\nabla\psi_{\mathrm{n}}(r,E,\hat{\Omega}) + \Sigma_{\mathrm{t}}(r,E)\psi_{\mathrm{n}}\left(r,E,\hat{\Omega}\right) &= \int_0^\infty\int_{4\pi}\Sigma_{\mathrm{s}}\left(E'\to E,\hat{\Omega}'\to\hat{\Omega}\right)\psi_{\mathrm{n}}\left(r,E',\hat{\Omega}'\right)d\hat{\Omega}'dE' + \\ &\frac{\chi(E)}{4\pi}\int_0^\infty\nu_{\mathrm{n}}(E')\Sigma_{\mathrm{f}}(r,E')\phi_{\mathrm{n}}(r,E')dE' + Q_{\mathrm{n}}\left(r,E,\hat{\Omega}\right),\end{aligned} \tag{3}$$

where

$$\mu_0 = \mu'\mu + [(1-\mu'^2)(1-\mu^2)]^{1/2}\cos\left(\varphi'-\varphi\right), \tag{4}$$

and where

$\hat{\Omega}$ = 3D unit vector

ψ_{e} = electron angular flux [$\mathrm{cm^{-2}\ s^{-1}\ sr^{-1}\ eV^{-1}}$]

σ_{t} = smooth-component total electron cross section [$\mathrm{cm^{-1}}$]

σ_{s} = smooth component scattering electron cross section [$\mathrm{cm^{-1}}$]

E = energy variable [eV]

μ = cosine of the directional polar angle

φ = directional azimuthal angle [rad]

α = restricted momentum transfer

S = restricted stopping power

Q_{e} = electron source distribution [$\mathrm{cm^{-3}\ s^{-1}\ sr^{-1}\ eV^{-1}}$].

ψ_{p} = photon angular flux [$\mathrm{cm^{-2}\ s^{-1}\ sr^{-1}\ eV^{-1}}$]

r = coordinate point in 3D space

μ_{t} = linear attenuation coefficient [$\mathrm{cm^{-1}}$] (includes γ,n reactions).

μ_{s} = photon scattering coefficient [$\mathrm{cm^{-1}}$]

R_{pf} = Photon gain rate term from photofission reactions [$\mathrm{cm^{-3}\ s^{-1}\ eV^{-1}}$]

Q_{p} = photon source distribution (includes bremsstrahlung and neutron fission gammas) [$\mathrm{cm^{-3}\ s^{-1}\ sr^{-1}\ eV^{-1}}$]

ψ_{n} = neutron angular flux [$\mathrm{cm^{-2}\ s^{-1}\ sr^{-1}\ eV^{-1}}$]

Σ_{t} = total macroscopic neutron cross section [$\mathrm{cm^{-1}}$]

Σ_{s} = scattering macroscopic neutron cross section [$\mathrm{cm^{-1}}$]

χ = Neutron fission energy spectrum

ν_{n} = average number of neutrons produced per fission

Σ_{f} = fission macroscopic neutron cross section [$\mathrm{cm^{-1}}$]

ϕ_{n} = Neutron scalar flux [$\mathrm{cm^{-2}\ s^{-1}\ eV^{-1}}$]

Q_{n} = neutron source distribution (includes photoneutrons) [$\mathrm{cm^{-3}\ s^{-1}\ sr^{-1}\ eV^{-1}}$]. (Morel 1996, Wang 2018, Duderstadt and Hamilton 1976)

The photofission term was extrapolated to be similar to a neutron fission term. The boundary conditions for the multiparticle (electron-photon-neutron) transport problem solved by MCNP are vacuum $\psi_e(r,E,\hat{\Omega}) = L(r,\hat{\Omega}) = \psi_n(r,E,\hat{\Omega}) = 0$ for $\hat{\Omega} \cdot \hat{e}_s < 0$ for all points r_s on boundary surface S_B. Also, Q_e is defined as a monodirectional and monoenergetic point source of electrons (to represent a narrow beam from the LINAC) with a strength of 7.2×10^{15} s^{-1} located near the left boundary of the problem. The SCALE ROM problem has similar vacuum boundary conditions $L(r,\hat{\Omega}) = \psi_n(r,E,\hat{\Omega}) = 0$ for $\hat{\Omega} \cdot \hat{e}_s < 0$ for all points within domain r_s on boundary surface S_B, except now the implicit source of radiation from the bremsstrahlung and photonuclear reactions in the LBE target (contained within Q_p and Q_n) in Equations (2–3) are precalculated.

The SCALE ROM's LBE source is calculated using F1 current tallies, i.e. number of particles, while voiding out all materials in the problem except the LBE target. F1 tallies were placed in two locations surrounding the LBE target to calculate the outgoing current and thereby characterize the relative distribution of particle solid angles and energies emitted from it. The first set of F1 tallies was placed on the outer surface of the LBE target (red outer surfaces in Figure 3) to estimate the total outward photon and neutron particle currents exiting the target.

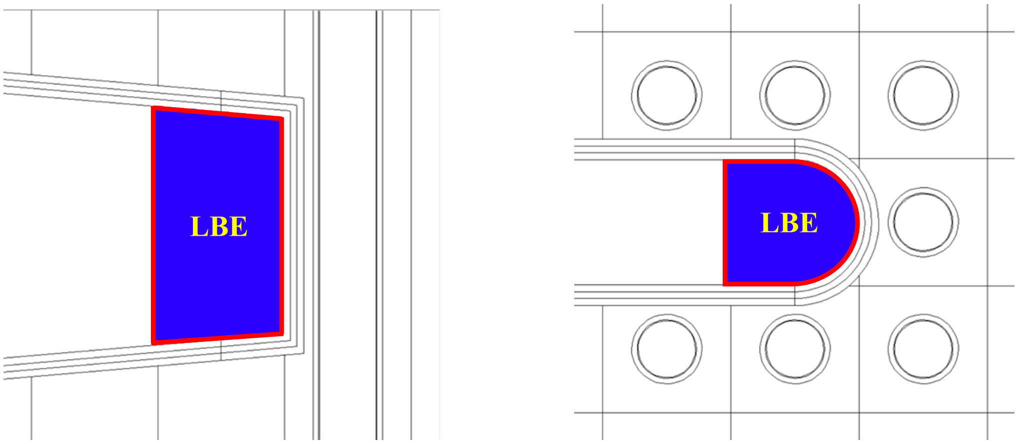

Vertical section

Horizontal section

Figure 3: Diagram of the F1 tally enclosure (red) of the LBE target used to calculate the total outgoing current.

The incoming electron rate provided by the Niowave LINAC specifications was 7.2×10^{15} s^{-1}. The total outgoing currents of photons and neutrons from the LBE target were found to be ~8.80×10^{15} s^{-1} (slight multiplication of photons) and 1.98×10^{13} s^{-1} (~1/500 photoneutron conversion efficiency), respectively. This is comparable to rates observed by Frankl and Macian-Juan for thick lead targets (Frankl and Macian-Juan 2016).

The second set of tallies were two long planes (200 m in both the y and z directions, also voiding out all materials except the LBE target). Planar F1 surface tallies placed at the positive and negative x-surfaces are shown in Figure 4.

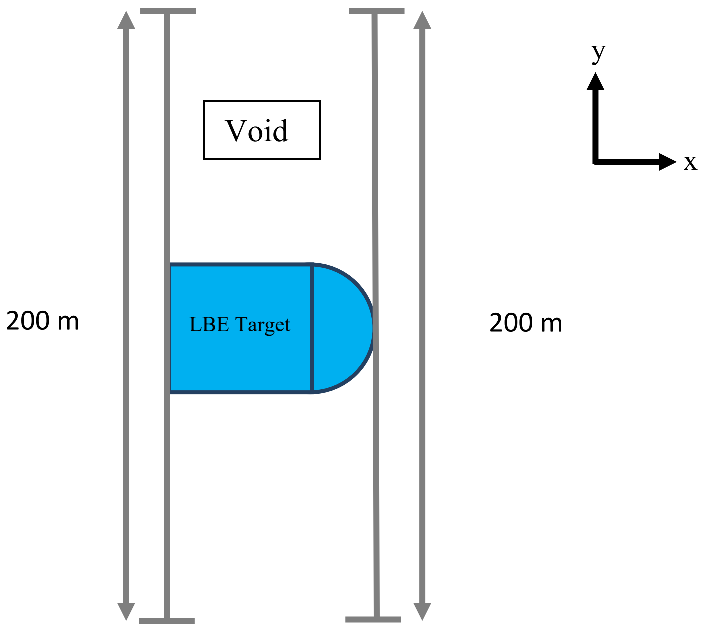

Figure 4: Diagram of 200 m MCNP F1 tally planes used to precalculate the outgoing currents from the LBE target for the SCALE ROM.

The two exceedingly long planes were chosen to reduce the complexity of the ROM from defining six planar sources to two, while still preserving most of the target's photon emissions. Further physics rationale for the choice of MCNP tallies is detailed in the following list of high-level assumptions.

The planar tally assumptions are that

- the target is thin compared with the length of the planes (the solid angle of photons that could escape from the simulation geometry without crossing these planes is small, about 5×10^{-6} % of the total 4π sphere area) and
- the bremsstrahlung produced by electrons "above a few MeV" tend to be "…confined to a very narrow forward beam," (Shultis and Faw 2000) so most of the higher energy photons should cross the long tallies.

However, note that the total current rate of the long planes is 20% and 22% lower than the previous LBE surface tally's rates for photons and neutrons, respectively. Therefore, although the leakage of particles in both the y- and z-directions is not negligible, it is a good starting place for replicating the x-axis dose. Ultimately, this ROM replicates the x-axis dose contributions well but does not fully capture the y and z dose contributions. Caution should be used when extrapolating to the y- and z-axis dose profiles near the ADSR.

The target was modeled bare (without a stainless-steel cover) in a void environment for simplicity. Each current tally was discretized by energy and cosine bins relative to the x-axis. A P_N-8 quadrature set (Lewis and Miller 1993) was selected for the angular bin structure, and the tally energy bin structure used is shown in Table 1.

Table 1. Energy bins utilized in the F1 current tally planar characterization of the LBE target source

Photon bin boundaries (eV)	Neutron bin boundaries (eV)

lower	0.0×10^{-3}
1	1.0×10^{6}
2	2.0×10^{6}
3	3.0×10^{6}
4	5.0×10^{6}
5	1.0×10^{7}
6	1.5×10^{7}
7	2.0×10^{7}

lower	1.0×10^{-5}
1	1.0×10^{0}
2	1.0×10^{3}
3	1.0×10^{4}
4	1.0×10^{5}
5	5.0×10^{5}
6	1.0×10^{6}
7	2.0×10^{6}
8	3.0×10^{6}
9	5.0×10^{6}
10	1.0×10^{7}
11	1.5×10^{7}
12	2.0×10^{7}

3.2 MAVRIC MODEL

Once the two F1 planar tallies were calculated by MCNP, a representative MAVRIC LBE source was defined. At first, energy and angularly averaged volume source geometries were considered for both the photon and neutron MAVRIC LBE source models. However, these geometries proved to be too simplistic to properly represent the anisotropy of the photon source (the primary contributor to external dose), and studies into the level of resolution required for accurate neutron emissions are continuing as well. Currently, the SCALE ROM consists of three components: two planar photon LBE sources (at the front and back of the target), a volumetric neutron LBE source, and a fission source (computed in KENO).

3.2.1 Photons

The spatial, angular, and energy data from the 200 m MCNP F1 tallies are collapsed into two much smaller planes (~3 × 6 cm) at the front and back of the LBE target in the MAVRIC ROM. A diagram of the ROM (Figure 5) and a list of modeling assumptions follow

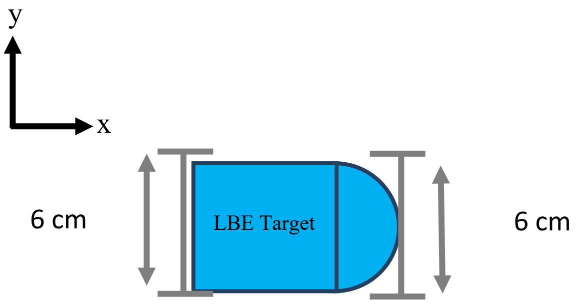

Figure 5: Diagram of two photon plane sources in front of and behind the LBE target, which represent the actual SCALE ROM LBE source.

The photon planar source ROM assumptions are that

- collapsing of the source planes to a much smaller emission plane will not substantially bias the angular and energy photon emission spectrums from the LBE target and
- the secondary photonuclear and photofission reactions lost along the y-axis will not significantly contribute to the x-axis dose.

A planar source representation is more advantageous than a volume because emitting from a volume source would require the LBE target cell to be filled with void to avoid significant photon scattering and attenuation. Voiding the LBE target would exclude secondary photoneutron interaction from occurring within the target from fission neutrons born inside the core. A drawback of using planar sources is that the leakage of photons from the LBE source at angles close to 90° in both the y- and z-directions is not captured in the MCNP tallying model, and those lost photons will be further amplified by not producing secondary photoneutrons and photofissions in the central column of uranium fuel pins.

The photon emission probability of the planar source ($w(E_g,\mu_k)$) for angle k is automatically converted into a probability density function by SCALE based on Equation (5).

$$w\left(E_g,\mu_k\right) = \frac{J^{\mathrm{p}}(E_g,\mu_k)}{\sum_{g=1}^{7} J^{\mathrm{p}}(E_g,\mu_k)} = \frac{J^{\mathrm{p}}(E_g,\mu_k)}{J^{\mathrm{p}}_{\mathrm{T},k}}, \tag{5}$$

where $J^{\mathrm{p}}\left(E_g,\mu_k\right)$ is the photon current $[\frac{\text{photons}}{\text{incident electron}}]$ tallied across the two planes in MCNP, E_g is the energy of group g, and μ_k, is the cosine of angle θ with respect to the x-axis and k=[1,9] for the angular bins, according to $\mathrm{P_N}$-8 quadrature.

The photon source strength, S_{p}, is normalized to the strength of the original LINAC electron source strength (see Equation [6]).

$$S_{\mathrm{p}} = (7.2 \times 10^{15}\ \mathrm{s}^{-1})\, J^{\mathrm{p}}_{\mathrm{T},k}. \tag{6}$$

The current weighted spectra emitted from two finite planes at the front and posterior x faces of the LBE target form the basis of the planar ROM.

The accuracy of the SCALE planar ROM can be investigated by including the ROM within a full UTA-2 ADSR core MAVRIC model (similar to Figure 2) and comparing it with the MCNP multiphysics core model. Figures 6 and 7 show the x-axis dose profile of the UTA-2 ADSR core at the center and along the $+y$-face of the core. Note, the diagrams in the upper right-hand corner are simple representations of the core for orientation only and do not accurately represent all aspects of the ADSR core geometry.

The MCNP and SCALE models agree to within 15% in dose magnitude at all locations outside of the target cell at the origin and agree well in shape overall. However, the MCNP photon dose is approximately an order of magnitude higher than the SCALE dose at the origin. This discrepancy is most likely an artifact of the internal target dose not being represented and from perpendicular photon emissions in both the y- and z-directions also not being represented by the ROM. An additional, small y-z narrow cone source should be considered as an ROM improvement to address this issue in future work. Also, note that the relative uncertainties for MCNP and SCALE are less than 1% and 5%, respectively, for all dose profiles in Section 3.2.1.

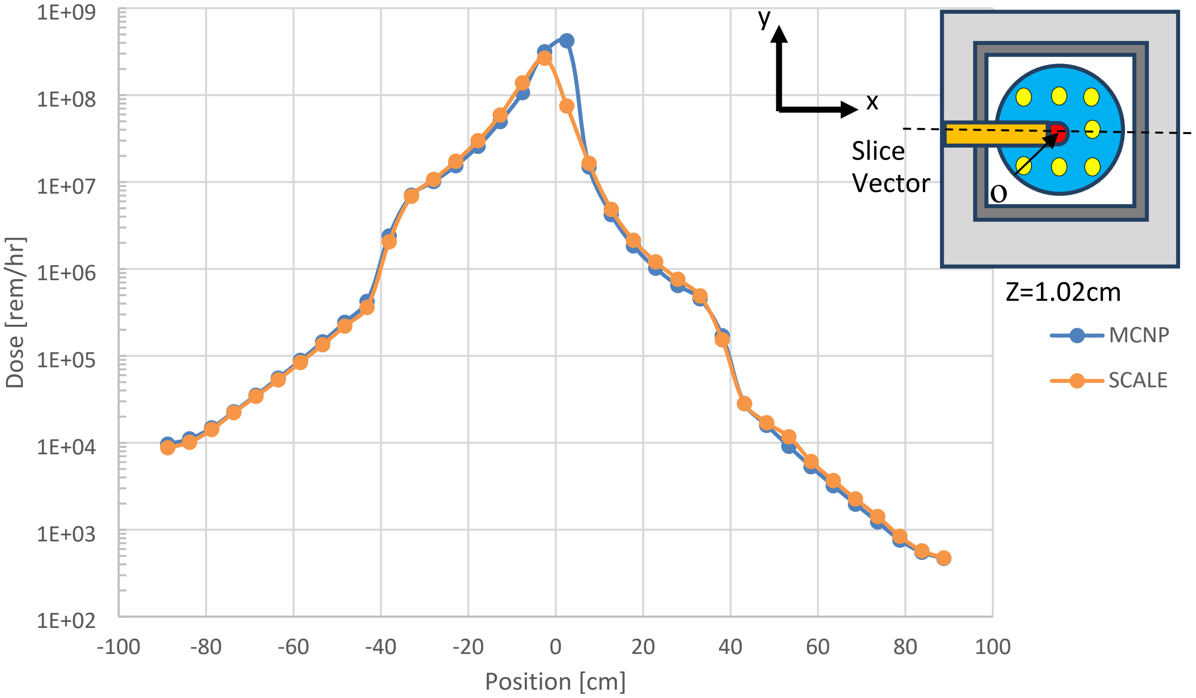

Figure 6: Photon dose profile along the x-axis of the UTA-2 ADSR core at y = 2.54 cm.

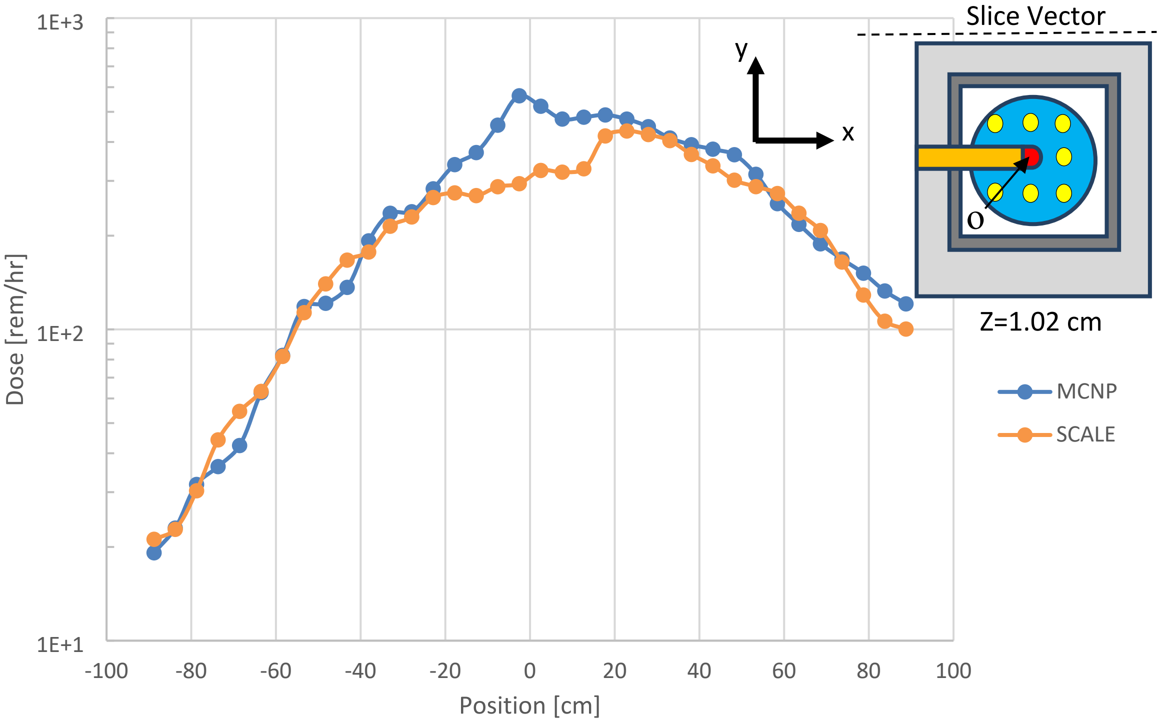

Figure 7: Photon dose profile in the x-direction of the UTA-2 ADSR core at y = 88.78 cm.

Examining the dose profile further from the center of the core still shows a larger discrepancy near the origin along the northern reactor wall; however, it is much less pronounced (48% maximum difference between MCNP and SCALE dose). Beyond ±20 cm, the dose profiles agree to within 25% and the shapes are in good agreement. These differences again allude to glancing angle emissions (nearly perpendicular to the x-axis) from the LBE target that are not being fully represented by the ROM, and likely those losses are amplified by not producing secondary photonuclear and photofission reactions in the central column of fuel pins.

Overall, the agreement in the x-profiles is encouraging because the area west of the reactor (parallel to the negative x-axis) has the greatest potential for photon leakage. Consider the prompt gamma ray energy spectrum emitted from U-235 in Figure 2 of the Maienschein report (Maienschein 1958). The large majority of prompt gamma rays are emitted below 4 MeV. Estimating a rough total fission rate of 7.18×10^{12} s^{-1} from the Niowave's UTA-2 power operating specification of 230 W and multiplying it by 0.1 MeV^{-1} and by 4 MeV equals ~2.87×10^{12}—4 MeV prompt gamma rays per second. Compare this to an average bremsstrahlung photon yield of 0.496 (estimated from Equation 6.14 in Turner for 20 MeV electrons in lead) (Turner 2007). Therefore, with an intensity of LINAC 20 MeV monoenergetic electrons impingent upon the LBE target of 7.2×10^{15} s^{-1}, this translates into a powerful point photon source of ~7.34×10^{15} s^{-1} with an average energy of 9.92 MeV.

Consequently, the LBE source is approximately three orders of magnitude higher in intensity and nearly 6 MeV higher in average energy. Again, Shultis and Faw state that higher energy bremsstrahlung photons will tend to be more forward biased (Shultis and Faw 2000) along the same direction of the original LINAC electron beam. Therefore, the highest dose area will be directly across from the LBE target on the western (negative x) side of the reactor.

Similar trends and levels of agreement were observed for the y-axis profiles and for the centerline z-axis profile. The differences did not exceed 38% and 47% for the y profiles and z centerline profile, respectively, and dose discrepancies continued to dissipate farther from the center of the reactor. The z-profile at the western edge of the reactor, however, showed a few additional differences (Figure 8).

MCNP and SCALE show more marked differences in shape for the western wall z-direction profile, and the magnitude in dose differences is up to 62%. One can observe that the SCALE profile is broader than the MCNP profile. It is suspected that this is an artifact of using too coarse of an angular discretization and that increasing the quadrature to P_N-16 could narrow the curve.

3.2.2 Neutrons

The MAVRIC LBE neutron source is represented separately from the photon source by a volume source for two reasons. First, it was assumed that by being the product of two particle interactions the neutron angular flux distribution would be more isotropic. Second, because fast neutrons are relatively blind to thin high-Z materials, it was assumed that neutron scattering and absorptions would have a negligible effect on the LBE neutron source spectrum. A diagram of the MAVRIC neutron LBE source structure is displayed in Figure 9.

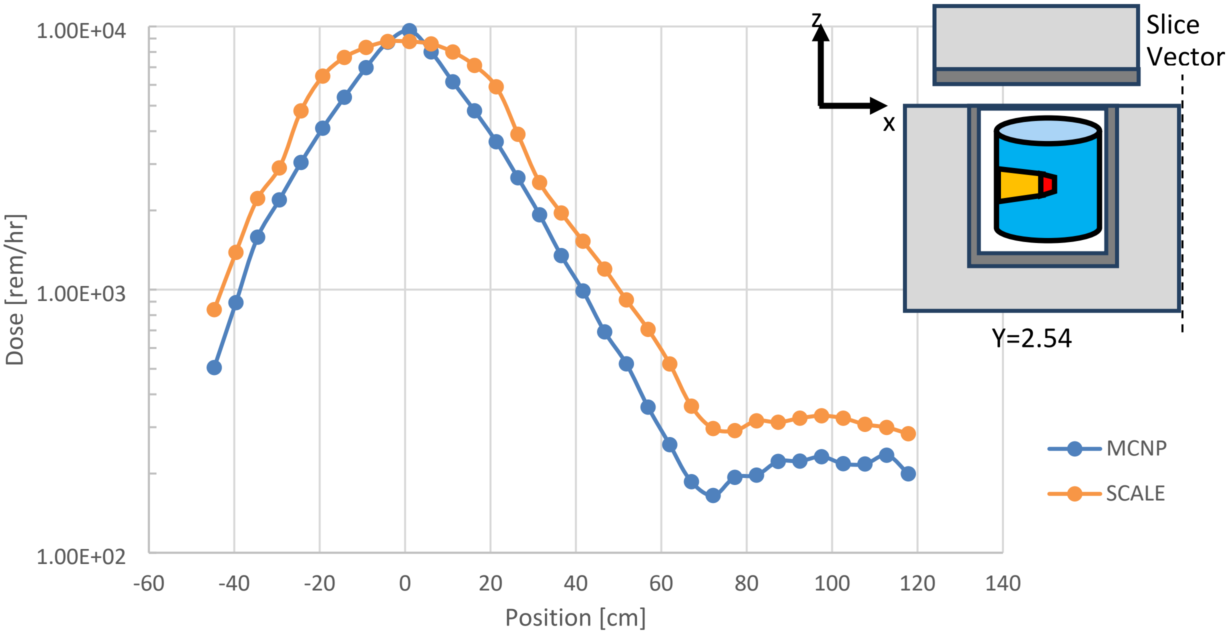

Figure 8: Photon dose profile in the z-direction of the UTA-2 ADSR core at x = -88.78 cm. *The fuel rods are not depicted in this schematic.

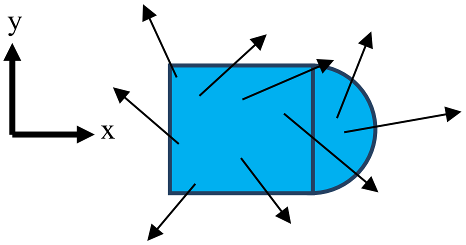

Figure 9: Diagram of MAVRIC neutron LBE volume source.

Unlike the MAVRIC photon planar energy distribution weighting (Equation [5]), the neutron volume source is a simpler distribution based off an averaged energy and angular weighting distribution (Equations [7] and [8]).

$$w(\mathrm{E_g}) = \frac{\sum_{k=1}^{9} J^{\mathrm{n}}(E_g,\mu_k)}{\sum_{\mathrm{k}=1}^{9}\sum_{g=1}^{12} J^{n}(E_g,\mu_k)} = \frac{\sum_{k=1}^{9} J^{\mathrm{n}}(E_g,\mu_k)}{J_{\mathrm{T}}^{\mathrm{n}}}. \qquad (7)$$

$$w(\mu_k) = \frac{\sum_{g=1}^{12} J^{\mathrm{n}}(E_g,\mu_k)}{\sum_{\mathrm{k}=1}^{9}\sum_{g=1}^{12} J^{\mathrm{n}}(E_g,\mu_k)} = \frac{\sum_{g=1}^{12} J^{\mathrm{n}}(E_g,\mu_k)}{J_{\mathrm{T}}^{\mathrm{n}}}. \qquad (8)$$

The neutron source strength is again normalized to the electron source strength (Equation [9]).

$$S_\mathrm{n} = (7.2 \times 10^{15}\ \mathrm{s}^{-1})\, J_\mathrm{T}^\mathrm{n}, \tag{6}$$

where $J^\mathrm{n}(E_g,\mu_k)$ is the neutron current $[\frac{\text{neutrons}}{\text{incident electron}}]$ tallied across the two planes in MCNP. Together, the energy and angular weights allow MAVRIC to sample an average neutron LBE source ROM from the target volume. Additionally, several assumptions were made during creation of the MAVRIC neutron ROM and are listed as follows.

The neutron volume source ROM assumptions are:

- The fast neutron energy spectrum produced by photonuclear reactions within the LBE target will be relatively insensitive to significant self-attenuation. The Pb and Bi neutron absorption cross sections are less than 100 mb for energies greater than 100 keV (LANL 2011).
- The angular distribution of neutron currents precalculated by MCNP is isotropic enough to not be significantly biased by additional scattering within the LBE target volume.
- Uniform fuel pin lattice resonance self-shielding (RSS) treatment of multi-group cross-sections in KENO is appropriate.

Figure 10 compares the x-axis centerline neutron dose profiles computed by MCNP and MAVRIC.

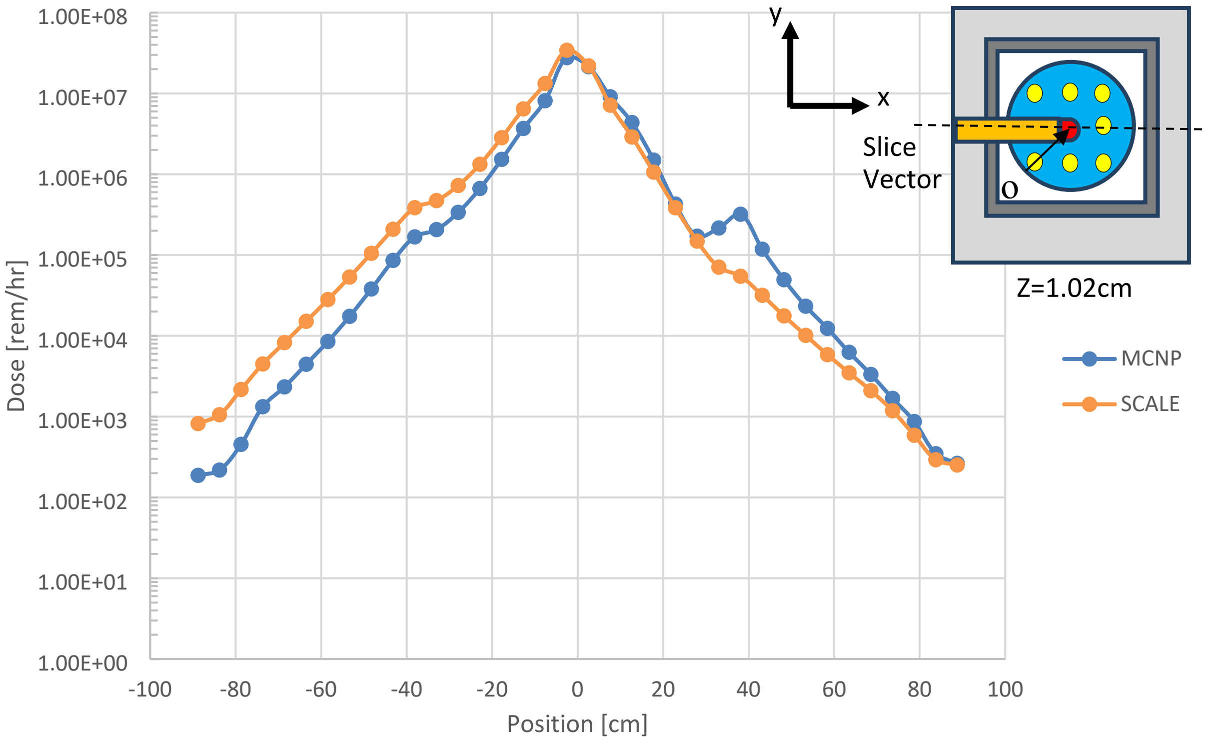

Figure 10: Neutron dose profile along the x-axis of the UTA-2 ADSR core at y = 2.54 cm.

The SCALE neutron volume ROM does not perform as well as the photon model. There are noticeable differences in shape and nearly a 50% difference in intensity in some regions. The relative uncertainties do not exceed 12% and 4% for the MCNP and SCALE models, respectively.

Several possible explanations for the discrepancies observed between the neutron SCALE ROM and MCNP multiphysics models are being explored. First, the geometry and input assumptions were examined carefully for both the SCALE ROM and the MCNP multiphysics model. No major differences were found except in the choice of cross section libraries and the treatment of RSS effects.
Cross section library differences were examined by running a simple 2 MeV point neutron surrogate source in place of the LBE source. The point source was placed inside the LBE target at the origin, and all the fissile uranium fuel materials were replaced by tantalum. MCNP and SCALE dose tallies produced values within two standard deviations of each other in each material region, eliminating cross section library differences as a source of inaccuracy.

Direct differences between the SCALE LBE ROM and the MCNP multiphysics LBE dose can be examined by voiding out all other geometry in both models. Comparative mesh tallies along the x-axis are displayed in Figure 11.

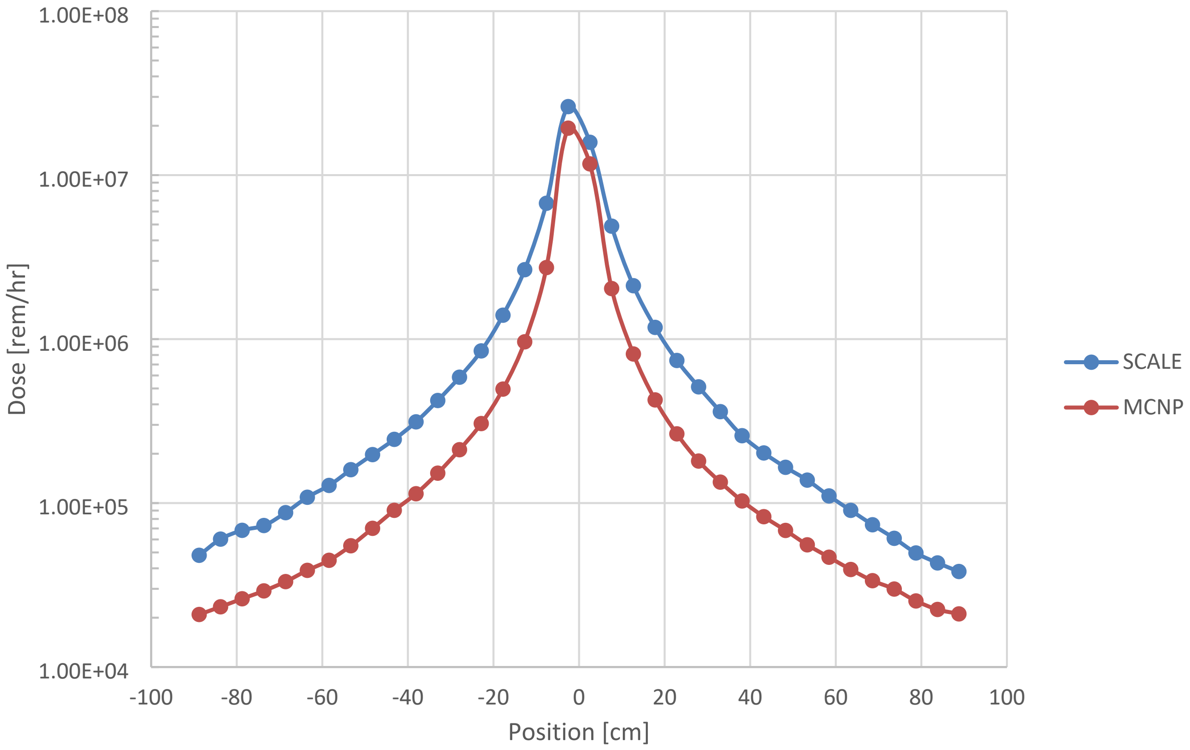

Figure 11: Void geometry neutron dose profile along the x-axis of the UTA-2 ADSR core at y = 2.54 cm.

The differences between the SCALE ROM model and the MCNP multiphysics model are only 27% in this case, and the shapes match with a slight backwards preference in the neutron source emission direction. This difference alone is unlikely to account for the full discrepancy shown previously in the full reactor geometry simulations (Figure 10); however, it is likely that this difference could be amplified by the fissile fuel around the source from both the neutron and photon LBE source (including photofission). Therefore, increased complexity and further refinement of the neutron ROM will be explored alongside refinement of the photon ROM in future work.

The current levels of accuracy in both the photon and neutron models are acceptable for preliminary facility radiation shielding calculations and design for two reasons. First, as noted in Section 3.2.1, the LBE target photon source emissions should be strongest along the x-axis, particularly in the forward direction (projected away from the beamline). Second, the photon LBE source accounts for 93% of the UTA-2 ADSR dose and the remaining 7% of neutron contributions are shared between the LBE (2%) and fission sources (5%).

Recall that the emission rates estimated from the MCNP multiphysics model in Section 3.1 showed that the photon emission rate was 1000 times larger than the neutron rate. Accounting for a 5-20 quality factor importance of neutron dose, the LBE neutron source would account for a maximum of 1/50th of the LBE photon source flux (which is more forward biased and generally higher in energy). Neutrons from fission will account for the other 5% of the total dose profile, assuming that an ~230 W power level (provided by Niowave design specification), 200 MeV per fission, and a standard emission of 2.43 neutrons per fission U-235 (according to Duderstadt and Hamilton [1976]) yields a total neutron emission rate of 1.74×10^{13} s^{-1}. This would account to closer to 1/20th of the total dose.

3.2.2.1 MAVRIC Fission Source

The SCALE package allows the calculation of a fission neutron source term through CSAS6/KENO, which can reduce computation time involved with particle tracking and multiplication (splitting) of neutrons in a shielding calculation. KENO runs a k-eigenvalue Monte Carlo calculation to calculate the fission rates and outputs the fission rate on a Cartesian mesh. Next, MAVRIC uses the "fission rate multiplied by the value of $\bar{\nu}$ to produce a fission neutron source (Wieselquist 2020). Additionally, prompt fission photons are generated during MAVRIC particle transport whenever imported fission neutrons interact within a fissile material in the model, even if the fission neutrons are disabled by users. Note that the total fission rate was normalized to previous rates calculated using the UTA-2 ADSR MCNP multiphysics model core optimization models (Karriem 2021).

Using a precalculated fission source in MAVRIC is advantageous for highly multiplying systems ($k_{\text{eff}}{\sim}1$) because traditional Monte Carlo methods must bank and track each neutron produced from fission. As k_{eff} approaches one, these fission chains of neutrons become lengthy and require a large amount of computation time to track to completion (i.e., leakage or absorption). Although the UTA-2 ADSR core is still fairly subcritical ($k_{\text{eff}} = 0.63$ from Niowave specifications), it will become more important for acceleration of the UTA-3 ADSR core model, which is projected to have a k_{eff} of 0.95.

Another consideration for acceleration of the method is the appropriateness of continuing to utilize multigroup cross section libraries over continuous energy libraries, when a beamline hole is present in the center of the UTA-2 fuel lattice and a secondary lattice of natural uranium fuel pins might invalidate the current uniform fuel lattice-based RSS assumption. For the SCALE KENO model with continuous energy cross sections, the k_{eff} was estimated at 0.70296 ($\pm$ 0.00016). With the default uniform pin lattice RSS assumption, the k_{eff} was originally equal to 0.69738 ($\pm$ 0.00012). This represents a difference of 558 pcm when accounting for proper RSS treatment. The MCNP model of the UTA-2 core yielded a k_{eff} of 0.70391 ($\pm$ 0.00013) or 95 pcm higher than the SCALE continuous-energy model. The differences in the k_{eff} values calculated (for the continuous energy cross section models) are nearly within overlapping uncertainty bounds of two standard deviations. While an improved RSS treatment should be considered against continuous energy methods in future work, these small differences are unlikely to account for the discrepancy observed in Figure 10.

3.3 MAVRIC GEOMETRY

The MAVRIC shielding models were developed directly from 2D and 3D illustrations and CAD documents provided by Niowave. Dimensions of the MAVRIC models are representative of the provided documents, but generalizations are also made based on radiation transport practices. A high-level list of relevant material and geometry assumptions follow.

- Material assumptions
    - All bulk materials (i.e., soil, sand, concrete, air) are considered perfectly homogenized and completely filling all volumes to which they are assigned. No attempt to model inhomogeneities was made.
    - Site soil assumes no water.
    - Site sand assumes 7% water concentration.
    - Site concrete is assumed to be reinforced concrete (i.e., includes high concentrations of iron).

- Geometry assumptions
    - Stairwell design is simplified (i.e., 10 cm concrete slanted surface instead of individual steps).
    - Potential structural steel or other components are not inside concrete walls (outside of homogenized structural concrete material assumptions).
    - Features and components of outer-facility walls and supports are simplified.

Given these assumptions, the site layout geometry was constructed encompassing a volumetric envelope of approximately 48 × 47 × 10 m (~22,500 m^3). Figure 12 shows various projections, perspectives, and layers of pertinent portions of the radiation transport model.

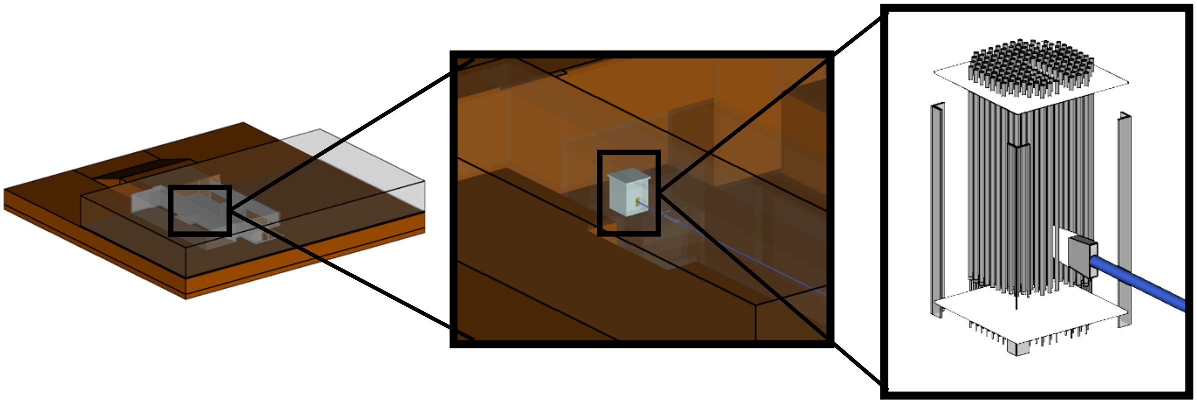

Figure 12: MAVRIC radiation transport geometry for Niowave's UTA-2 Airport Facility in full isometric (left), subterranean reactor/beamline area (middle), and reactor core (right).

Subsections of the MAVRIC model were developed in parallel and made possible by the compartmentalized capability of SCALE's geometry framework. The SCALE Standard Geometry Package (SGGP) not only allows the same model to be shared between two different SCALE sequences (i.e., KENO and MAVRIC) but also provides a unique feature used in this work: the concept of a *hole*. A hole (with regard to SGGP nomenclature) is a process of inserting an independent subsection of a geometry called a *unit* into the greater *global unit*. This allowed the analysts to, in parallel, develop a detailed reactor model and a site layout model independently and then combine the two (i.e., via making a *hole*) for a complete radiation transport model (Figure 13).

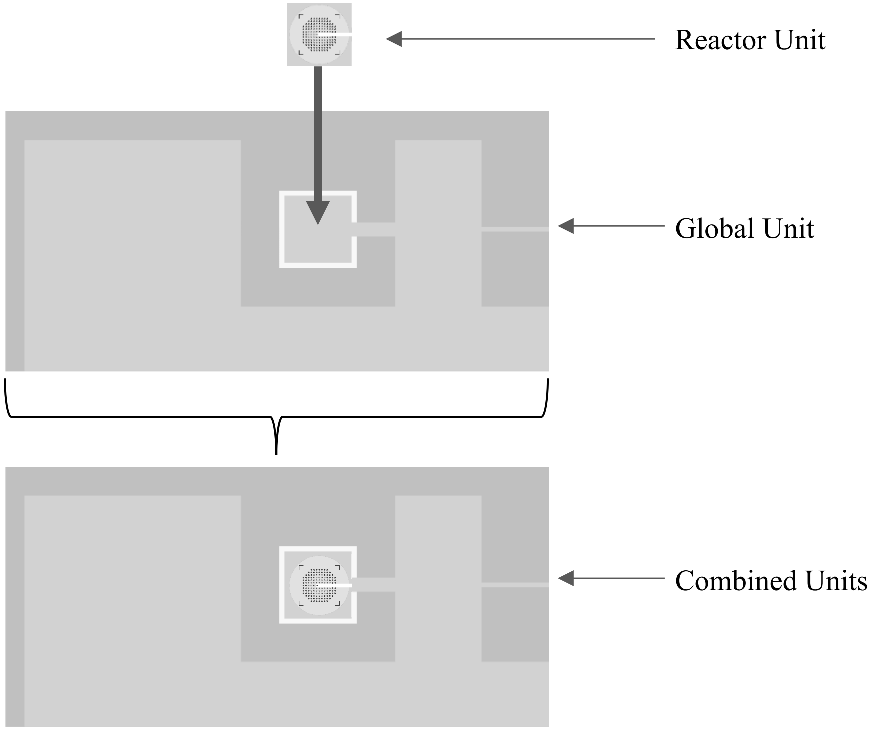

Figure 13: Illustration of combining various units of the geometry in parallel before performing simulations.

3.3.1 MAVRIC Tallies

The MAVRIC calculations use Cartesian grid meshes for assessing the effective dose rate (rem/hour) implications throughout the facility. This is done by taking the global unit and subdividing it into smaller volumetric pixels—or *voxels.* Once a simulation is started, each voxel serves as an individual energy-dependent particle tally. Each voxel of the mesh tally computes the flux using the average pathlength of particle tracks divided by the voxel volume. These tallies are automatically normalized to source strength, and any multipliers that are used to appropriately weight the respective tally to the source particle activity. During the calculation, the energy-dependent flux is also convolved with the response functions, such as the full body effective dose rate to a human. This analysis used the 1977 American National Standards Institute standard flux-to-dose conversion factors for photons and neutrons separately to generate results in rem h^{-1} for each (ANS 1977) and then combined the two tallies in postprocessing to estimate the implications of the total mixed radiation field. Efforts to further subdivide source contributions from LBE vs fission were not made.

Although unoptimized—or *analog*—Monte Carlo calculations are extremely efficient at sampling billions of particle interactions, it can be extremely difficult to populate voxels in heavily shielded regions of a geometry without leveraging variance reduction methods. MAVRIC allows users to relatively easily perform adjoint calculations, importance map generation, and source term weighting to get particles carrying the most influence to the regions of the problem of highest interest (Peplow 2011). For these reasons, populating all regions (and thus all voxels) of a large geometry is not feasible in a single calculation, and multiple calculations are required to identify reasonable estimates of the dose rate in various locations with a high degree of confidence. Figure 14 qualitatively demonstrates the effects of biasing a simulation to various regions of the geometry.

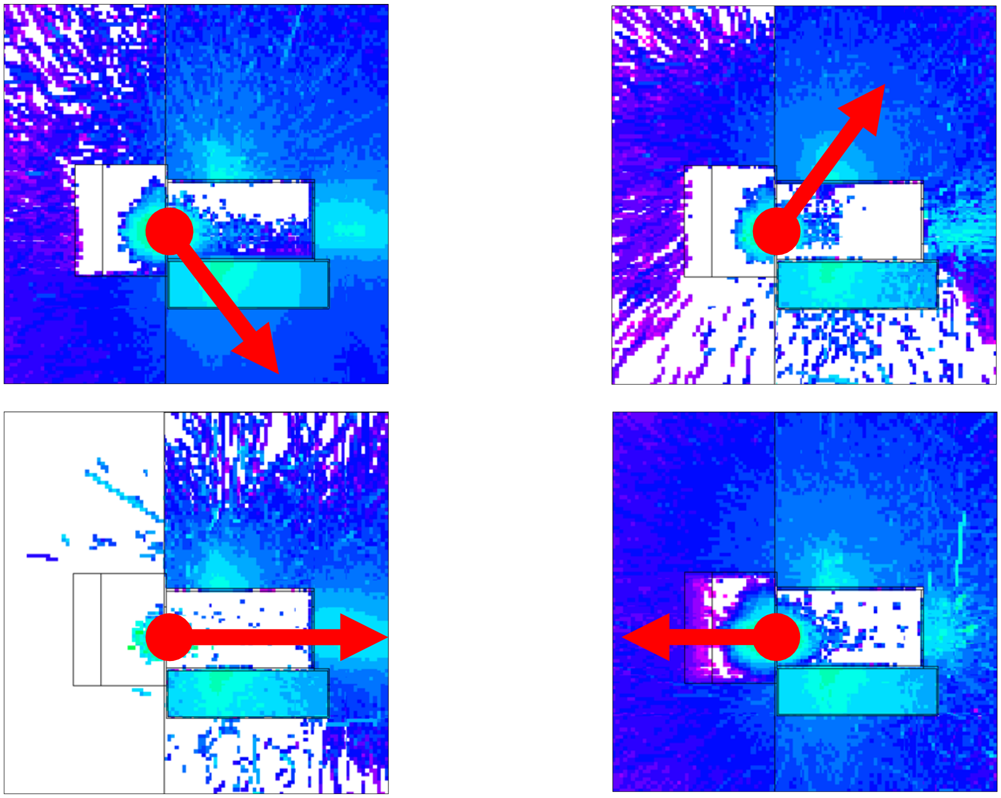

Figure 14 : Illustration of biasing particles in the MAVRIC simulation to four distinctly different regions of the geometry. Although colormaps are not provided for this qualitative comparison, the blue regions represent the intensity of dose rates, and the red arrows indicate the general direction of particle biasing for each simulation.

4. RESULTS

Niowave requested the use of specific locations within the UTA-2 facility for assessing the radiological impact during operations. These locations are enumerated in Figure 15.

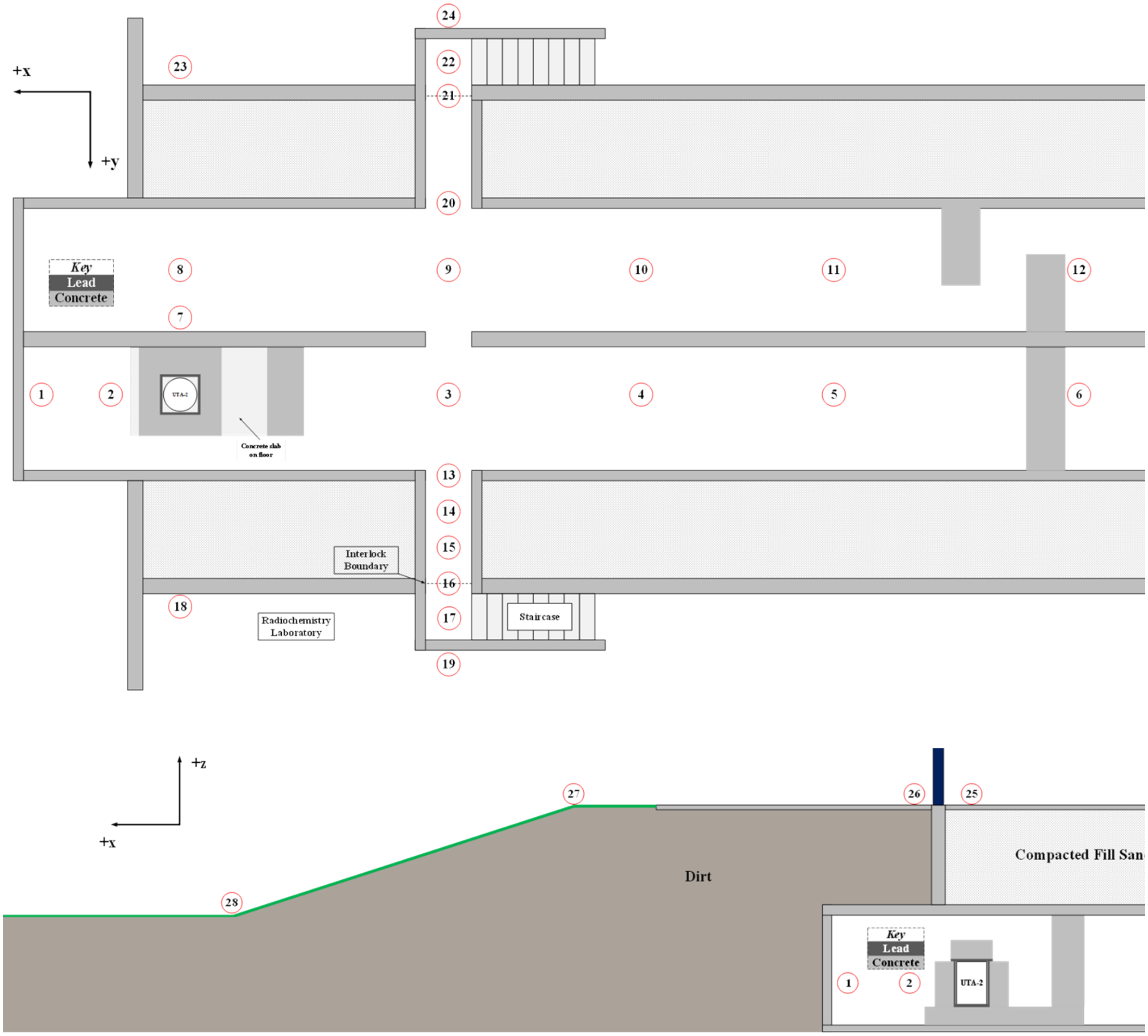

Figure 15: Illustration of the 28 requested locations throughout the UTA-2 Airport Facility. Top is a plane view of the second floor and bottom is an evaluation view through the reactor. Images courtesy of Niowave, Inc.

Many of the locations of interest in the tunnel areas near the accelerator and reactor could be estimated to low uncertainties with a single calculation because of the elevated radiation levels and comparatively low shielding materials. However, other deep penetration locations on the upper floors and outside the facility required additional, targeted calculations. Note that to provide a dose rate estimate for each requested location with less than 20% uncertainty, several separate calculations were performed.

Results from the radiation transport calculations are categorized into definitions outlined by the NRC and are tabulated in Table 2. This categorization is not necessarily what Niowave will employ or even be required to adhere to, but it is a means to communicate the hierarchy of the ambient radiation fields in a regulatory context. It is worthy of note that many nuclear facilities choose to restrict their exposure limits to levels that are more conservative than federal regulators require. The extent to which Niowave should limit their exposures beyond regulatory guidelines is not the purpose of this document, and suggestions of this type are not provided.

Table 2: NRC radiation exposure categories used to rank radiation transport results.

Area type	NRC limits	Reference
Very high radiation area	$\geq$ 500 rad h^{-1}	10 CFR 20.1003
High radiation area	$\geq$0.1 rem h^{-1} & <500 rad h^{-1}	10 CFR 20.1003
Radiation area	$\geq$0.005 rem h^{-1} & <0.1 rem h^{-1}	10 CFR 20.1003
Controlled area	$\geq$0.002 rem h^{-1} & <0.005 rem h^{-1}	10 CFR 20.1201 Subpart C
Uncontrolled area	<0.002 rem h^{-1}	10 CFR 20.1201 Subpart C

4.1 OCCUPATIONAL DOSE RATE RESULTS

Figure 16 shows cross-sectional dose maps of the upper and outside facility and the lower tunnel area. The tunnel's surrounding walls of concrete, soil, and sand effectively prevent penetration of radiation to much of the facility. The maps show dose rates ranging from kilorem h^{-1} (orange) near the reactor, to mrem h^{-1} (light blue) in the farthest distances in the tunnels, to µrem h^{-1} (dark blue) at the farthest distances outside the facility. Although these figures provide quantitative and qualitative insight into the ambient radiation of the operating facility, Table 2 provides detailed and tabulated dose rates corresponding to the exact locations of interest requested by Niowave. Discussion here is relegated to high-level dose rate implications.

Table 3: Facility dose values at locations specified in Figure 15.

Location Number	Dose (rem h^{-1})	Error (%)	NRC Area Type
1	681.08	0.5%	Very high radiation area
2	2,437.78	0.3%	Very high radiation area
3	7.57	2.4%	High radiation area
4	2.91	1.7%	High radiation area
5	1.65	13.2%	High radiation area
6	0.02	11.9%	Radiation area
7	8.37	1.0%	High radiation area
8	4.38	1.0%	High radiation area
9	0.44	14.3%	High radiation area
10	0.19	1.9%	High radiation area
11	0.03	2.8%	Radiation area
12	0.003	13.5%	Controlled area
13	1.97	3.9%	High radiation area
14	0.68	1.8%	High radiation area
15	0.26	2.0%	High radiation area
16	0.19	1.8%	High radiation area
17	0.11	1.8%	High radiation area
18	3.6×10^{-4}	12.3%	Uncontrolled area
19	0.003	9.0%	Controlled area
20	0.25	7.4%	High radiation area

21	0.05	5.7%	Radiation area
22	0.04	4.9%	Radiation area
23	3.8×10^{-5}	31.4%	Uncontrolled area
24	0.002	9.1%	Controlled area
25	5×10^{-4}	13.4%	Uncontrolled area
26	4×10^{-4}	7.6%	Uncontrolled area
27	4.5×10^{-6}	31.4%	Below background
28	8.7×10^{-8}	21.8%	Below background

During operation, dose rates in much of the tunnel will fall into a *high radiation* or even *very high radiation* category, which will require access control, radiation warnings (signs/alarms), and physical measures to prevent personnel from entering during operation. However, this analysis implies that much of the facility's upstairs locations can be considered *controlled* or even *uncontrolled areas* without additional shielding. It is suggested in later sections that additional shielding could lower the ambient operational radiation environment in everyday working areas to *uncontrolled* area levels. Efforts to shield these areas is advisable to adhere to the radiological philosophy of As Low As Reasonably Achievable (ALARA).

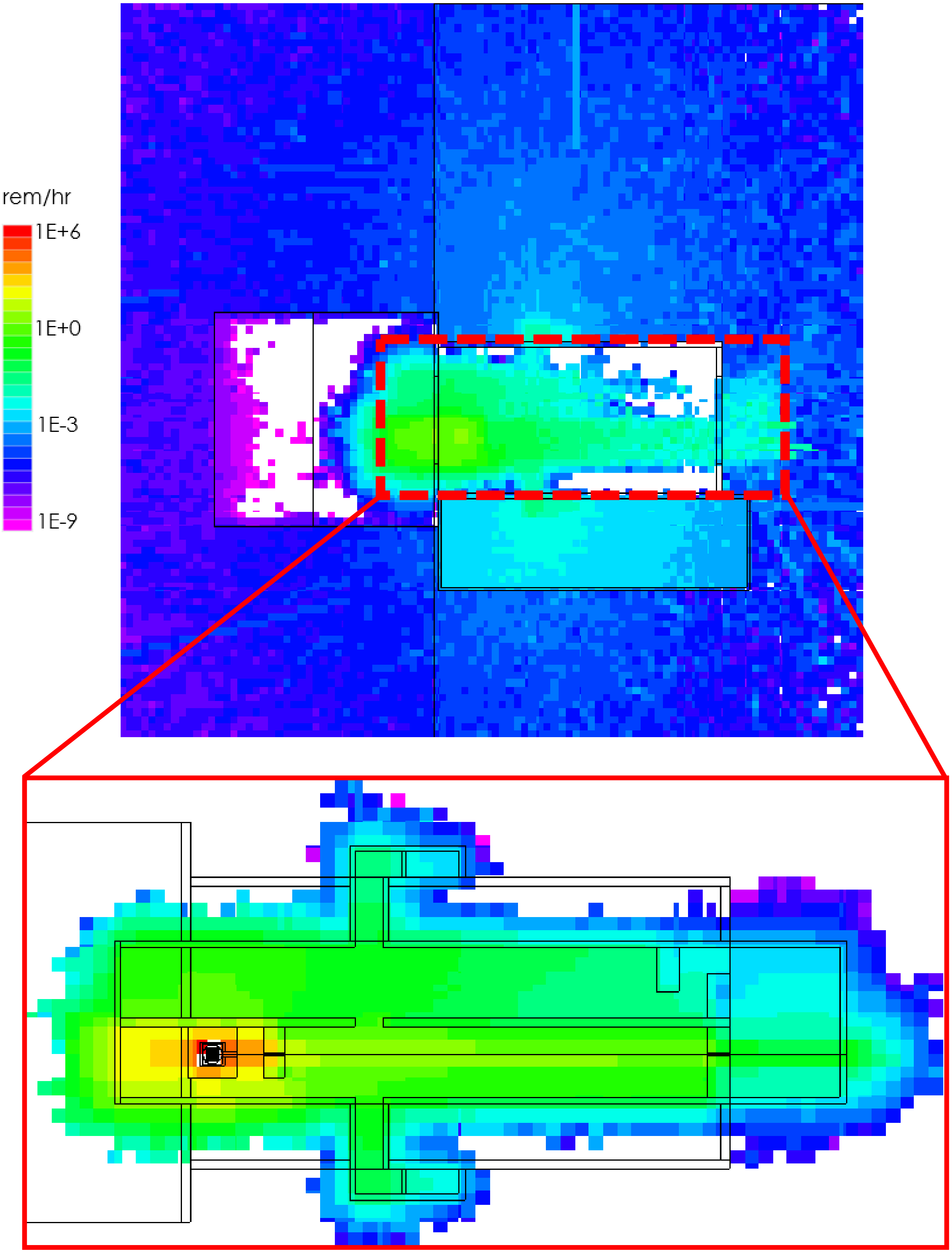

Figure 16: Dose rate maps of UTA-2 upper and outside areas (top), with zoom-in of lower tunnel areas (bottom).

4.2 OBSERVATIONS AND RECOMMENDATIONS

This section presents various observations and recommendations informed by the results of this analysis. Note, it is understood at this time that no personnel are intended to be in the tunnels during accelerator/reactor operation, and this analysis supports that decision as evidenced by dose rates in the tunnel areas, which are expected to range from ~0.1 – ~1000 rem h^{-1}. Furthermore, because these recommendations are informed by simulations alone, it is advised that Niowave confirm results of the radiation simulations via in-field ionizing radiation measurements before implementing any recommendations. The recommendations of this analysis team are as follows:

- Even while not under operation, because of the potential for lethal (or even elevated) exposures in the event of inadvertent operation of the accelerator/reactor while personnel are performing maintenance, personal protection systems (PPSs) are advised for all tunnel areas.
    - PPSs may include systems such as access control to areas using proximity cards, lock and key, lock-out-tag-out methods, and programmable logic controllers.
    - These systems should be coupled with formally developed, and regularly tested, safety procedures for all safety systems.
    - Before sealing a given area for operation, personnel should first sweep an area for occupants before locking out each compartmentalized area.
    - These systems should follow typical accelerator safety standards dictated by regulatory agencies such as DOE and the NRC.
- Dose rates near various access points to the tunnels will range from ~0.1 – ~1 rem h^{-1}, and these access points also provide avenues for radiation leakage into upstairs environments. It is recommended to implement additional, moveable shields to occlude these paths from the accelerator/reactor areas during operation. This will physically secure personnel from entering and prevent radiation from escaping to other areas while operating. Additionally, dose rates outside much of the facility appear to be well within the NRC limits to be qualified as uncontrolled areas. So, it is reasonable to assume that if the previous shielding strategies at tunnel access points are implemented, the controlled areas will likely decrease to uncontrolled areas as well.
- It is recommended that radiation area monitors be placed throughout the facility to monitor if/when abnormalities in shielding (sand, soil, concrete, etc.) develop as a result of construction or over time from operations.
- Although this analysis studied operational radiation sources, it did not include shutdown radiation sources that could present a nontrivial radiological hazard when the reactor/accelerator are not active, yet personnel are expected to be in and around the tunnel area. Radiological implications to personnel should be studied for the following nonoperational radioactive sources:
    - Fission products in spent fuel
    - Activated hardware on, in, and around the reactor/accelerator
    - Radioisotope products extracted from the reactor
- This analysis did include predominant operational sources (i.e., fission and LBE) but did not examine all potential sources during operation. Consideration in future investigations should include additional investigation of the following operational radioactive sources:

- Accelerator-induced radiation via beamline losses and bremsstrahlung
- Air and material activation around the reactor

5. CONCLUSION

The current analysis represents a preliminary look at the ambient radiation environment produced by the Niowave UTA-2 accelerator and reactor while operating. The SCALE ROM methodology was employed to accelerate calculations and reduce computational burdens on the project. The photon LBE ROM approximates the more computationally expensive MCNP multiphysics dose profile well along the x-axis but could benefit from further improvement along other profiles. Losses from fission photons appear to be significant. Unfortunately, the SCALE 6.2.4 package does not fully incorporate photonuclear physics, so further investigation into the relative contributions of photonuclear reactions to neutron dose need to be investigated before continuing development of the neutron LBE ROM. In fact, this will likely justify the selection of a different coupling between MCNP multiparticle physics and SCALE's accelerated radiation shielding engine in future work.

Although simulations suggest there are areas of extremely high occupational dose rates while in operation, simple strategies for access control can be implemented to prevent exposures in these elevated areas. Preliminary calculations in this document did not entertain additional shielding at tunnel access points. Some areas around these access points presented as *radiation areas* (i.e., <0.1 rem h^{-1}), but even without additional shielding, much of the facility can be classified as an *uncontrolled area* (i.e., <0.002 rem h^{-1}). Inclusion of additional shielding at tunnel access points can easily mitigate areas of elevated radiation, further decrease the overall radiation environment outside of the immediate tunnels, and adhere to the radiological philosophy of ALARA.

These radiation simulations of the current UTA-2, in the current airport facility design, imply that there are no abnormal radiation environments when compared with other similar nuclear facilities (i.e., nuclear reactors and accelerators). The layout appears to have sufficient in situ shielding to protect much of the facility during operation (given proper operational controls of personnel), but minimal additions of shielding in key locations can only improve the overall radiological implications to personnel.

6. REFERENCES

WNA. September 2020. “Advanced Nuclear Power Reactors.” Accessed December 31, 2020. https://www.world-nuclear.org/information-library/nuclear-fuel-cycle/nuclear-power-reactors/advanced-nuclear-power-reactors.aspx.

WNA. November 2020. “Small Nuclear Power Reactors.” Accessed December 31, 2020. https://www.world-nuclear.org/information-library/nuclear-fuel-cycle/nuclear-power-reactors/small-nuclear-power-reactors.aspx.

NNSA. 2019. “NNSA’s Molybdenum-99 Program: Establishing a Reliable Supply of Mo-99 Produced Without Highly Enriched Uranium.” Accessed December 31, 2020. https://www.energy.gov/nnsa/nnsa-s-molybdenum-99-program-establishing-reliable-supply-mo-99-produced-without-highly.

IAEA. 2001. *IAEA Safeguards Glossary*. Vienna, Austria: International Atomic Energy Agency.

Makarashvili, V., Chemerisov, S., and Micklich, B. 2012. “Simulations of a LINAC-based photoneutron source.” *Nucl. Instrum. Methods Phys. Res. A*, vol. 696: 136–140.

Tatari, M., and Ranjbar, A. H. 2014. “Design of a photoneutron source based on 10 MeV electrons of radiotherapy linac.” *Ann. Nucl. Energy*, vol. 63: 69–74.

He, M., et al. 2015. “Beam transient analyses of Accelerator Driven Subcritical Reactors based on neutron transport method.” *Nucl. Eng. Des.*, vol. 295: 489–499.

IAEA. 1974. *Handbook on Nuclear Activation Cross-Sections: Photonuclear Cross-sections.* Technical Report 156. International Atomic Energy Association.

M. Bencomo. 2016. “Parametric Study of Mo-99 Production Using a Subcritical Low Enriched Uranium Assembly Design Proposed by Niowave Inc.” Master’s Thesis, College Station, TX: Texas A&M University.

Morel, J. E., et al. 1996. “A Hybrid Multigroup/Continuous-Energy Monte Carlo Method for Solving the Boltzmann-Fokker- Planck Equation.” *Nucl. Sci. Eng.*, vol. 124: 369–389.

Wang, A., et al. 2018. “A fast, linear Boltzmann transport equation solver for computed tomography dose calculation (Acuros CTD).” *MEDICAL PHYSICS*, vol. 46, iss. 2: 925-933. https://doi.org/10.1002/mp.13305.

Duderstadt, J., and Hamilton, L., 1976. *Nuclear Reactor Analysis*. Ann Arbor, Michigan: John Wiley & Sons.

Frankl, M., and Macian-Juan, R., May 2016. “Photonuclear benchmarks of C, Al, Cu, Ta, Pb, and U from the ENDF/B-VII cross-section library ENDF7U using MCNPX.” *Nucl. Sci. Eng.*, vol. 183, no. 1. https://doi: 10.13182/NSE15-47.

Shultis, J. K., and Faw, R. E. 2000. *Radiation Shielding*. La Grange Park, IL: American Nuclear Society.

Lewis, E. E., and Miller, W. F. Jr. 1993. *Computational Methods of Neutron Transport*. La Grange Park, IL: American Nuclear Society.

Maienschein, F. C., et al. June 1958. *Gamma Rays Associated With Fission*. A/CONF.15/P/670. pp. 670–686. https://doi.org/10.2172/4325517.

Turner, J. 2007. *Atoms, Radiation, and Radiation Protection*, 3rd ed. Weinheim, Germany: Wiley-VCH.

LANL. 2011. “Evaluated Nuclear Data Files (ENDF) Data.” Los Alamos National Laboratory. Accessed January 1, 2021. https://t2.lanl.gov/nis/data/endf/endfvii.1-n.html.

Wieselquist, W. A., Lefebvre, R. A., and Jessee, M. A. April 2020. *SCALE Code System*. Manual ORNL/TM-2005/39. Oak Ridge: Oak Ridge National Laboratory.

Karriem, Z., et al. 2021. *Neutronic Sensitivity and Optimization Analysis for Design Phase 2 of the Niowave Uranium Target Assembly (UTA-2) for Molydenum-99 Production*. ORNL/TM-2021/2250. Oak Ridge: Oak Ridge National Laboratory.

ANS. 1977. *American National Standard: Neutron and Gamma-Ray Flux-to-Dose Rate Factors (1977)*. Standard ANSI/ANS 6.1.1-1977. LaGrange Park, Illinois: American Nuclear Society.

Peplow, D. E. May 2011. "Monte Carlo Shielding Analysis Capabilities With MAVRIC." *Nucl. Technol.* 174(2), 289-313